Nano Research

Open Access

Research Article

Excellent microwave absorption performance of polyphenol-metal coordination derived magnetic porous carbon spheres

Jing Dang[1] ✉ and Panbo Liu[2]

[1] China AVIC the First Aircraft Institute, Yanliang 710089, China
[2] School of Chemistry and Chemical Engineering, Northwestern Polytechnical University, Xi'an 710129, China

Cite this article: *Nano Research*, **2025**, *18*, 94907032. https://doi.org/10.26599/NR.2025.94907032

ABSTRACT: Electromagnetic synergy and porous characteristics are two dominant factors in realizing light-weight and high-efficient microwave absorption performance. In this paper, a formaldehyde-assisted metal-ligand crosslinking strategy and a subsequent pyrolysis process are employed to synthesize magnetic porous carbon spheres with the electromagnetic synergy and porous characteristics, in which metal ions are tightly anchored in poly-(tannin acid) spheres because of the strong chelation coordination between them. The chemical composition of magnetic particles and the microwave absorption performance of the derived magnetic porous carbon spheres can be manipulated by adjusting the metal ions. Benefiting from the cooperative effects of porous structure, matched impedance, the electromagnetic synergistic enhancement between magnetic particles and carbon matrix, as well as the improved interfacial polarization caused by the large number of hetero-interfaces, both the microwave absorption intensity and the effective absorption bandwidths are significantly enhanced for magnetic porous carbon spheres, such as Co-PCSs and CoNi-PCSs, compared with PCSs. With 15 wt.% filler loading, the maximum reflection loss of CoNi-PCSs is −51 dB at 2.2 mm and the effective bandwidth is 7.2 GHz at 2.9 mm. Furthermore, this study provides the theoretical theory for the design and development of light-weight and highly efficient microwave absorption materials.

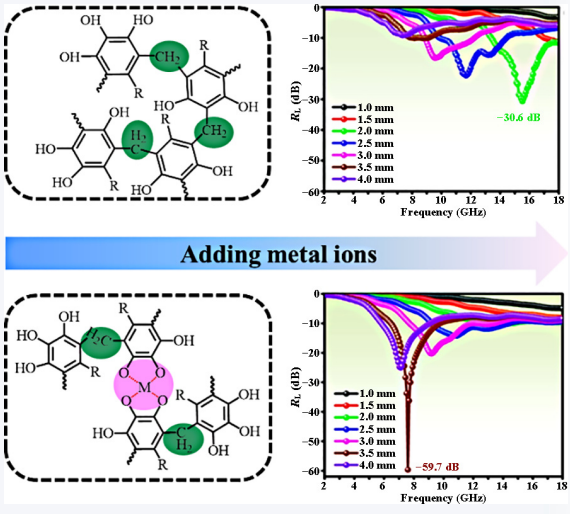

KEYWORDS: chelation coordination, porous structure, magnetic particles, electromagnetic synergy, microwave absorption performance

1 Introduction

Rapid development of radar detection technology and widespread use of electronic communication equipment have seriously threatened stealth characteristics of weapons and normal use of instrumentation equipment. Therefore, there is an urgent need to develop microwave absorption materials to solve the mentioned above problems. Ideal microwave absorption materials should possess following characteristics, such as thin thickness, light weight, strong absorption and wide frequency band [1, 2].

Compared with traditional ferrite-based absorbents, carbon materials possess the characteristics of light weight, thin thickness and good stability, which have potential application in the field of microwave absorption [3, 4]. However, the dielectric constants of carbon materials are usually high, resulting in mismatched impedance. Electromagnetic waves are easy to reflect on the surface of the matrix, and could not be absorbed by the inside materials [5]. Furthermore, carbon materials only exhibit simple dielectric loss mechanism for electromagnetic wave absorption, which makes them difficult to achieve both strong absorption and wide bandwidths [6]. It is well known that microwave absorption properties of carbon materials are closely related to their chemical compositions and microstructures. Therefore, researchers are devoted to improving microwave absorption performances of carbon materials by two kinds of methods [7, 8]. One is to combine magnetic particles with carbon materials to improve the impedance matching of carbon materials, which makes carbon materials

Received: July 22, 2024; **Revised:** August 3, 2024
Accepted: August 8, 2024

✉Address correspondence to dangjing1985@163.com

possess both dielectric loss and magnetic loss [9, 10]. The second strategy is to prepare carbon materials with porous structure, which can significantly reduce dielectric constants of carbon materials and improve the impedance matching [11, 12]. The introduction of porous structure can also change microwave propagation path of materials, further enhancing the microwave absorption performance. Han et al. [13] prepared Co@C microspheres with core-shell structure by coating phenolic resin outside and high temperature carbonization process. The carbon layers coating not only reduced the conductivity of microspheres and introduced interfacial polarization, but also suppressed the skinning effect generated by the Co crosslinking co-network, resulting in stronger magnetic loss. Its maximum reflection loss was −68.7 dB, which was higher than that of the single Co particle (−18.9 dB).

Metal-organic frameworks (MOFs) are materials with porous structures constructed by metal ions and organic ligands through coordination. Recently, pyrolysis process has been employed to prepare MOFs derived microwave absorption materials with electromagnetic synergism, which has attracted much attention, and the effective combination of porous structure and electromagnetic synergism can be achieved by the design of metal ions and organic ligands after carbonization [14, 15]. Firstly, metal ions can be easily reduced to magnetic metals or magnetic metal oxides by high temperature carbonization and embedded inside the carbon matrix to form core-shell structure, which is conducive to enhancing interfacial polarization and improving dielectric loss [16]. Secondly, the magnetic loss and microwave absorption properties of the carbide can be modulated through the selection of metal ions [17]. Yang et al. [18] constructed CoFe@C@MnO_2 hierarchical nano cubes with multi-heterogeneous interfacial core-shell structures by a multi-step method. Because the matched impedance, multiple interface polarization and the electromagnetic synergy, the derived absorbents exhibited the maximum reflection loss of −64 dB at 1.3 mm and an effective bandwidth of 9.2 GHz at 1.6 mm. Compared with MOFs-derived microwave absorbents, biomass materials own wide source, abundant resources and low cost in nature, and their unique porous tissues still maintain the certain pore structure after carbonization, which can be used to prepare porous carbon microwave absorption materials. Li et al. [19] compared electromagnetic wave absorption properties of various biomass-derived porous carbons and found that microwave absorption performance of the multi-layer porous carbon obtained by high-temperature carbonization of spinach was the best, but its absorption performance mainly originated from dielectric loss. To improve the impedance matching and effective frequency bandwidth, Meng et al. [20] introduced magnetic particles Fe_3O_4@Fe into the three-dimensional porous carbon obtained by carbonization of loofah sponge, and the resulting composite materials exhibited effective absorption bandwidth of 5.0 GHz with thickness of 2 mm. Above studies have shown that biomass tissues contain a large amount of plant polyphenols. Their unique chemical structures have a strong chelation and coordination effect with metal ions. After carbonization, magnetic doped porous carbon can be formed to achieve the integration of electromagnetic loss of biomass-derived carbon materials. However, the above works have not conducted further investigation on this issue.

In this study, by taking the advantage of strong chelation and coordination interaction between tannic acid molecules and metal ions (Co^{2+}, Co^{2+}+Ni^{2+}), magnetic porous carbon sphere composites with the electromagnetic synergy and porous structure are prepared through the formaldehyde-assisted ligand crosslinking and high-temperature carbonization strategies, which providing a reference for the design and preparation of lightweight and efficient microwave absorption materials.

2 Experimental sections

2.1 Materials

Ammonia (concentration of 35%), formaldehyde (concentration of 37%), $Co(NO_3)_2{\cdot}6H_2O$ (analytical purity), and $Ni(NO_3)_2{\cdot}6H_2O$ (analytical purity) were purchased from Shanghai Macklin Biochemical Co., Ltd. Anhydrous ethanol (analytical purity) was received from Tianjin Fuyu Fine Chemical Co., Ltd. Tannic acid (concentration of 95%) was purchased from Shanghai Aladdin Biochemical Technology Co., Ltd.

2.2 Preparation of PCSs, Co-PCSs and CoNi-PCSs

The synthesized process is illustrated as follows: (1) 0.6 mL of ammonia was added to a mixed solution of 12 mL of deionized water and 53 mL of absolute ethanol, and the mixed solution was stirred for 10 min. (2) 233 mg of tannic acid was added and stirred for 30 min. (3) 0.4 mL of formaldehyde solution was added and stirred for 2 h. (4) 233 mg of tannic acid and 0.4 mL of formaldehyde solution were added and stirred for 24 h. (5) After centrifugal washing for several times, the obtained product was placed in an oven and kept at 200 °C for 2 h. (6) The obtained product was placed in a tube furnace, and calcined at 800 °C for 2 h under nitrogen protection, with the heating rate of 5 °C/min, to obtain derived porous carbon spheres, named as PCSs. In step (4), 300 mg of $Co(NO_3)_2{\cdot}6H_2O$ was added and other steps are unchanged to obtain cobalt particle-doped magnetic porous carbon spheres, named as Co-PCSs. Similarly, in step (4), 150 mg of $Co(NO_3)_2{\cdot}6H_2O$ and 150 mg of $Ni(NO_3)_2{\cdot}6H_2O$ were respectively added, and other steps are unchanged to obtain cobalt-nickel particle-doped magnetic porous carbon spheres, named as CoNi-PCSs. The preparation process is shown in Fig. 1.

2.3 Characterizations

The morphologies of samples were characterized by the Verios G4 scanning electron microscope (SEM) and the Talos F200X transmission electron microscope (TEM). The lattice of samples was analyzed by the Ultima IV X-ray diffraction (XRD, Cu-Kα radiation). The carbon element structures in samples were analyzed by the Alpha 300R Raman spectrometer. The specific surface areas and pore size distributions of samples were analyzed by Sorp–Mini specific surface area analyzer. The magnetic properties of samples were analyzed by the CFMS-14T multifunctional physical property measurement system (PPMS). The electromagnetic parameters of samples were tested by 3672A/B/C-S vector network analyzer, and the coaxial method was used. The paraffin and samples (85:15) were fully mixed and then pressed into a ring with the outer diameter of 7.0 mm and an inner diameter of 3.0 mm for testing.

3 Results and discussion

3.1 Morphological analyses

Figures 2(a)–2(f) exhibit the microscopic morphologies of poly-(tannin acid) spheres, Co^{2+}/poly-(tannin acid) spheres, and

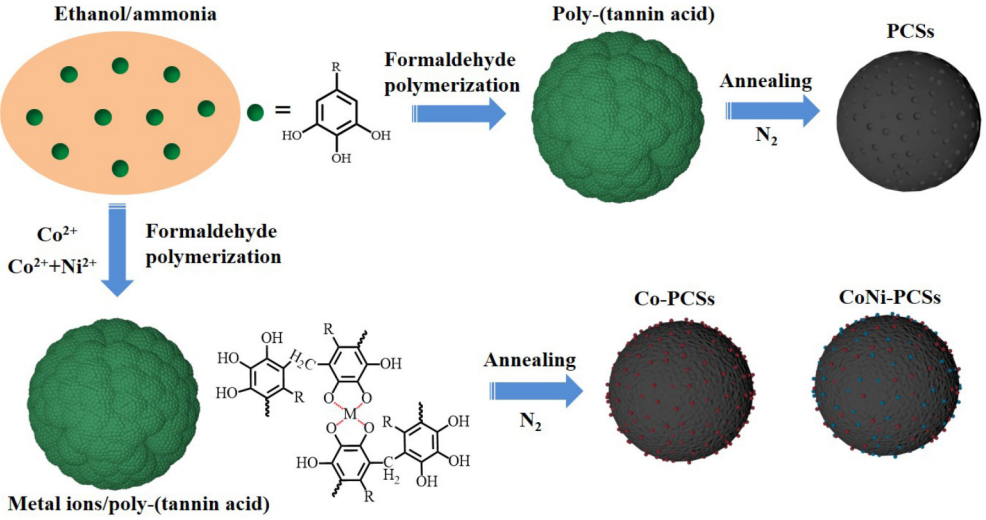

Figure 1 Preparation process of PCSs, Co-PCSs and CoNi-PCSs.

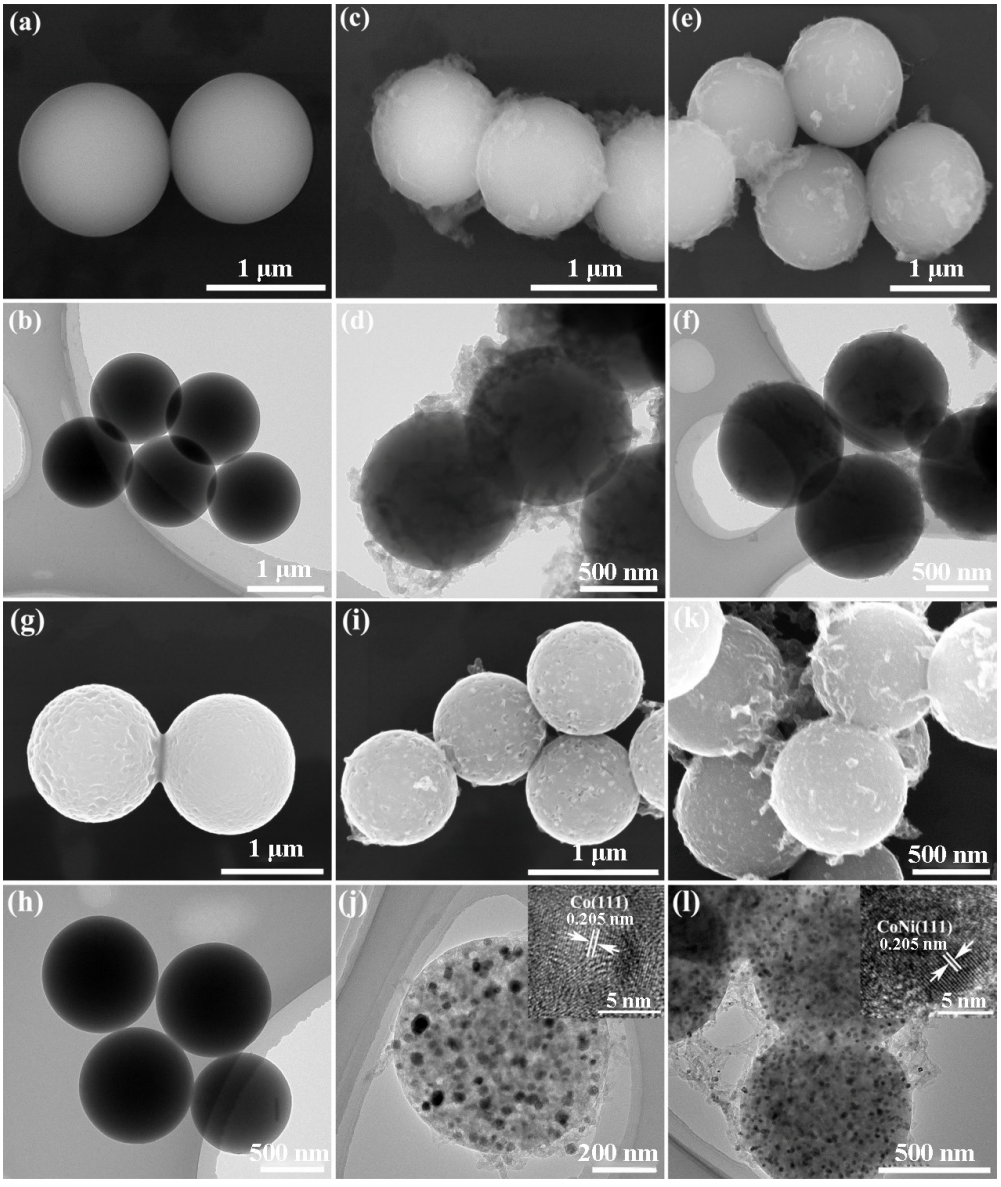

Figure 2 SEM and TEM images of poly-(tannin acid) spheres (a) and (b), Co^{2+}/poly-(tannin acid) spheres (c) and (d), $Co^{2+}Ni^{2+}$/poly-(tannin acid) spheres (e) and (f), PCSs (g) and (h), Co-PCSs (i) and (j) and CoNi-PCSs (k) and (l).

$Co^{2+}Ni^{2+}$/poly-(tannin acid) spheres, respectively. From Figs. 2(a) and 2(b), it can be observed that poly-(tannin acid) spheres fabricated via the formaldehyde-assisted ligand cross-linking strategy feature smooth surface and homogeneous size distribution. Upon the addition of metal ions, the surface of the formed Co^{2+}/poly-(tannin acid) spheres (Figs. 2(c) and 2(d)) and $Co^{2+}Ni^{2+}$/poly-(tannin acid) spheres (Figs. 2(e) and 2(f)) become rough, and the particle size increases in contrast to the poly-(tannin acid) spheres, indicating that the metal ions are adsorbed within the poly-(tannin acid) spheres through the chelation coordination. It is known that when the reduction potential of metal ions is larger or close to −0.27 V, metal ions are preferred to reduce to magnetic particles after the high-temperature carbonization. When the reduction potential of metal ions is significantly lower than −0.27 V, the products at high-temperature carbonization are typically metal oxides [21]. Therefore, under the protection of inert gas and calcination at 800 °C, the product resulting from high-temperature calcination of poly-(tannin acid) spheres is PCSs, the product of Co^{2+}/poly-(tannin acid) spheres is Co-PCSs (Co^{2+}→Co), and the product of $Co^{2+}Ni^{2+}$/poly-(tannin acid) spheres is CoNi-PCSs (Co^{2+}+Ni^{2+}→CoNi). The chemical composition of magnetic particles can be modified by adjusting the types of chelation-coordinated metal ions. Figures 2(g)–2(l) exhibit the SEM and TEM images of PCSs, Co-PCSs, and CoNi-PCSs, respectively. As shown in Figs. 2(g) and 2(h), PCSs formed after high-temperature carbonization still possess the spherical structure, but the surface becomes coarse and the color contrast is uniform, suggesting the absence of magnetic particles in PCSs. For Co-PCSs (Figs. 2(i) and 2(j)) and CoNi-PCSs (Figs. 2(k) and 2(l)), distinct dark particle areas emerge in the corresponding transmission photos, indicating the presence of magnetic particles. Compared with PCSs, magnetic particles are conducive to enhancing the magnetic loss of materials and thereby improving the impedance matching. Additionally, both the metal Co particles and CoNi particles are small, forming more heterogeneous interfaces with carbon matrix, which is beneficial for enhancing the interface polarization.

3.2 Compositional analyses

Figure 3 shows the XRD spectra of PCSs, Co-PCSs and CoNi-PCSs, respectively. As shown in Fig. 3, PCSs show a distinct diffraction peak centered at about 25°, corresponding to the characteristic peak of carbon matrix. Co-PCSs show the distinct diffraction peaks at 44.3°, 51.6° and 75.8°, respectively, corresponding to the (111), (200) and (220) crystal planes of metallic Co, indicating that the chemical composition of this particle is Co. The diffraction peaks of CoNi-PCSs display a good match with metallic Co and metallic Ni, indicating that the particles are CoNi alloys.

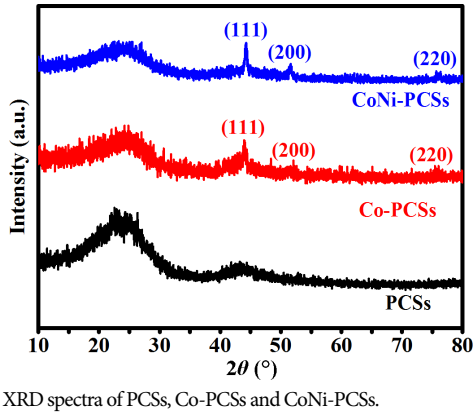

Figure 3 XRD spectra of PCSs, Co-PCSs and CoNi-PCSs.

The carbon components in PCSs, Co-PCSs, and CoNi-PCSs are analyzed by Raman spectroscopy, and the results are shown in Fig. 4. Generally speaking, the Raman spectra of carbon matrix usually have two distinct peaks, located at 1348 (D peak) and 1589 cm^{-1} (G peak), respectively. The D peak is mainly caused by the defects or lattice distortions of carbon atoms, while the G peak mainly originates from the planar stretching vibration of sp^2 carbon atoms. Therefore, the relative intensity ratio of the D peak to the G peak (I_D/I_G) can be used to indirectly reflect the graphitization degree of carbon matrix. A larger value of I_D/I_G indicates the presence of more defects or lattice distortions in the carbon matrix after high-temperature carbonization. Conversely, a smaller value of I_D/I_G suggests the higher graphitization degree in the carbon matrix materials. As shown in Fig. 4, the values of I_D/I_G in Co-PCSs and CoNi-PCSs are 0.92 and 0.89, respectively, both lower than that of PCSs (0.96), indicating that the carbon structure in PCSs has more defects. This is mainly due to the certain catalytic effect of the magnetic particles formed after high-temperature carbonization. During the high-temperature carbonization process, the graphitization degree of carbon structure is greatly improved, resulting in reducing I_D/I_G value.

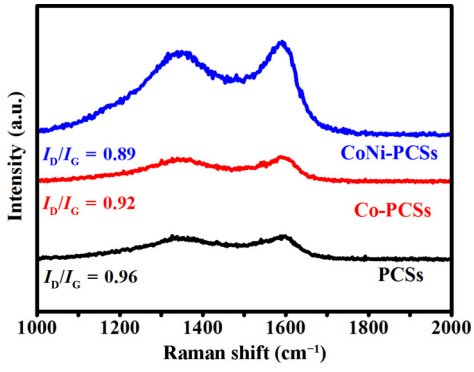

Figure 4 Raman spectra of PCSs, Co-PCSs and CoNi-PCSs.

3.3 Analyses of specific surface area

The specific surface areas and pore size distributions of PCSs, Co-PCSs and CoNi-PCSs are analyzed by N_2-adsorption-desorption curves in Fig. 5. As can be seen, the adsorption-desorption curves of all samples show the significant growth trend at a relatively low pressure (P/P_0 < 0.1), indicating the existence of microporous structures. In addition, in the relative pressure of 0.4–0.9, the hysteresis loops of Co-PCSs and CoNi-PCSs are different from that of PCSs, and their typical IV curves indicate the existence of obvious mesoporous structures. From the above analyses, it can be concluded that PCSs, Co-PCSs and CoNi-PCSs possess microporous-mesoporous characteristics. Besides, it is clear that the mesoporous characteristics of Co-PCSs and CoNi-PCSs are more obvious, which is consistent with the results of their pore size distributions. The optimal pore size of PCSs is 3.8 nm, and the pore size distribution shows a significant increase trend in the microporous region. The optimal pore sizes of Co-PCSs and CoNi-PCSs are about 3.7 nm. According to the BET method, the specific surface areas and pore volumes of PCSs, Co-PCSs and CoNi-PCSs are 430.86 and 0.11, 322.49 and 0.32, 415.26 and 0.26 cm^3/g, respectively. The specific surface areas of Co-PCSs and CoNi-PCSs are lower than that of PCSs, which is related to their optimal mesoporous characteristics. Therefore, their pore volumes are higher than that of PCSs. For porous materials, higher specific

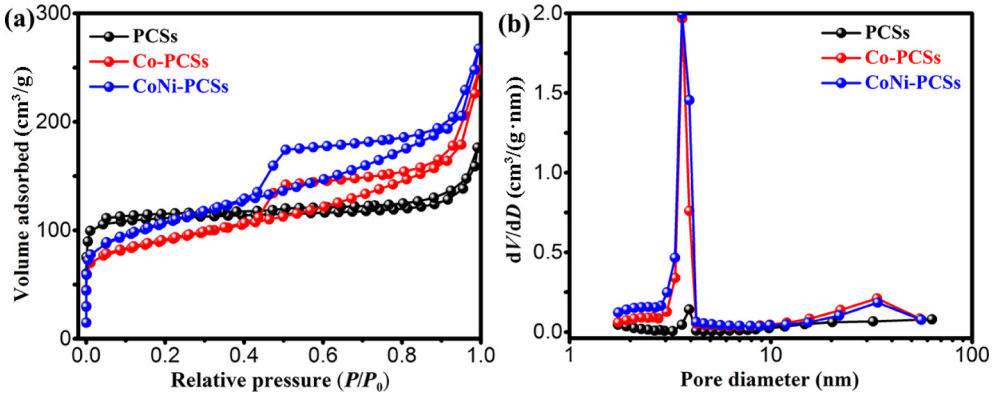

Figure 5 N_2 absorption–desorption isotherm (a) and pore size distribution (b) of PCSs, Co-PCSs and CoNi-PCSs.

surface area can not only increase the multiple scattering of electromagnetic waves, but are also helpful to reduce the filling amount of absorbers and can be used as the lightweight and efficient microwave absorber.

3.4 Analyses of magnetic properties

The magnetic properties of Co-PCSs and CoNi-PCSs are analyzed by VSM respectively, and the hysteresis curves are shown in Fig. 6. The PCSs obtained by high-temperature calcination are non-magnetic substances and do not have obvious magnetic loss performance, while the magnetic losses of Co-PCSs and CoNi-PCSs mainly come from the internal magnetic Co particles and CoNi particles. As can be seen from Fig. 6, hysteresis curves of Co-PCSs and CoNi-PCSs both present S-shaped curves, showing superparamagnetic characteristics. Their saturation magnetization and coercivity are 12.63 emu/g and 109.2 Oe, 12.97 emu/g and 48.2 Oe, respectively. The differences in saturation magnetization and coercivity are mainly due to the differences in size, crystallinity and content of magnetic particles. Compared with PCSs, the existence of magnetic particles not only introduces magnetic loss in materials, but also improves the impedance matching of materials through electromagnetic synergy, further improving microwave absorption performance of the materials [22].

3.5 Analyses of microwave absorption performances

As shown in Fig. 7, the maximum reflection loss (R_L) and the effective absorption frequency bandwidths of PCSs, Co-PCSs and CoNi-PCSs are analyzed through the line transmission theory, in which the filling amount of absorbents is 15 wt.%. R_L is calculated using Eqs. (1) and (2)

$$Z_{in} = Z_0\sqrt{\mu_r/\varepsilon_r}\tan\left[j(2\pi fd/c)\sqrt{\mu_r/\varepsilon_r}\right] \quad (1)$$

$$R_L(\mathrm{dB}) = 20\log_{10}|(Z_{in}-Z_0)/(Z_{in}+Z_0)| \quad (2)$$

where μ_r represents the relative complex permeability, ε_r represents the complex permittivity, f stands for the frequency of electromagnetic waves in vacuum conditions, d represents the thickness of the microwave absorption materials and c is the speed of light. From Figs. 7(a) and 7(b), it can be observed that when the thickness is 2 mm, the minimum reflection loss for PCSs is only −30.6 dB, and the effective absorption bandwidth lower than −10 dB is 5.5 GHz at 2.3 mm. Because there are no magnetic components, thus the microwave absorption of PCSs mainly stems from the dielectric dissipation. It is known that incorporating magnetic particles into carbon materials can enhance the microwave absorption performance through the electromagnetic synergy and multi-loss synergy mechanisms [23]. Therefore, in contrast to PCSs, both the microwave absorption intensity and the effective absorption bandwidths of Co-PCSs and CoNi-PCSs are increased. As shown in Figs. 7(c) and 7(d), the maximum reflection loss of Co-PCSs has a significant enhancement compared with PCSs. When the thickness is 3.7 mm, the minimum reflection loss is up to −59.7 dB, and the effective absorption bandwidth exhibits a marginal increase, achieving 5.6 GHz at 2.9 mm. As depicted in Figs. 7(e) and 7(f), for CoNi-PCSs, both the minimum reflection loss and the effective absorption bandwidth have manifested a marked improvement compared with PCSs. When the thickness is 2.2 mm, the minimum reflection loss of CoNi-PCSs is −51 dB, and the effective absorption bandwidth can attain 7.2 GHz at 2.9 mm.

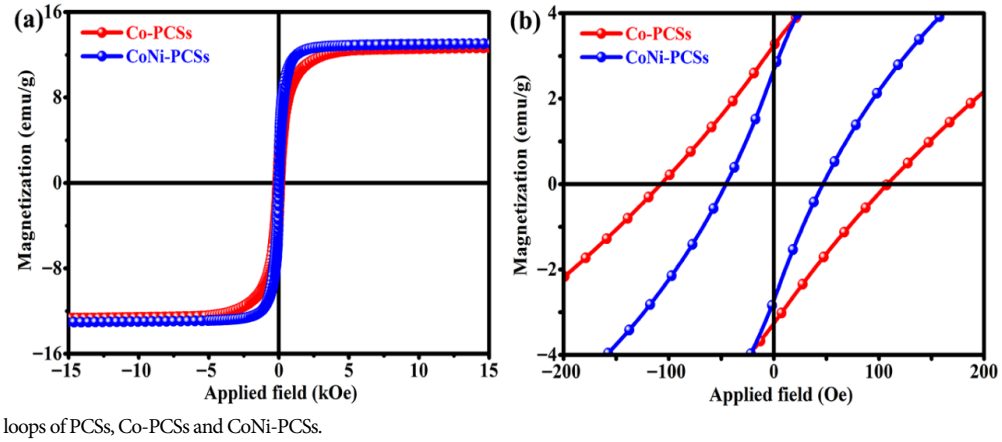

Figure 6 Hysteresis loops of PCSs, Co-PCSs and CoNi-PCSs.

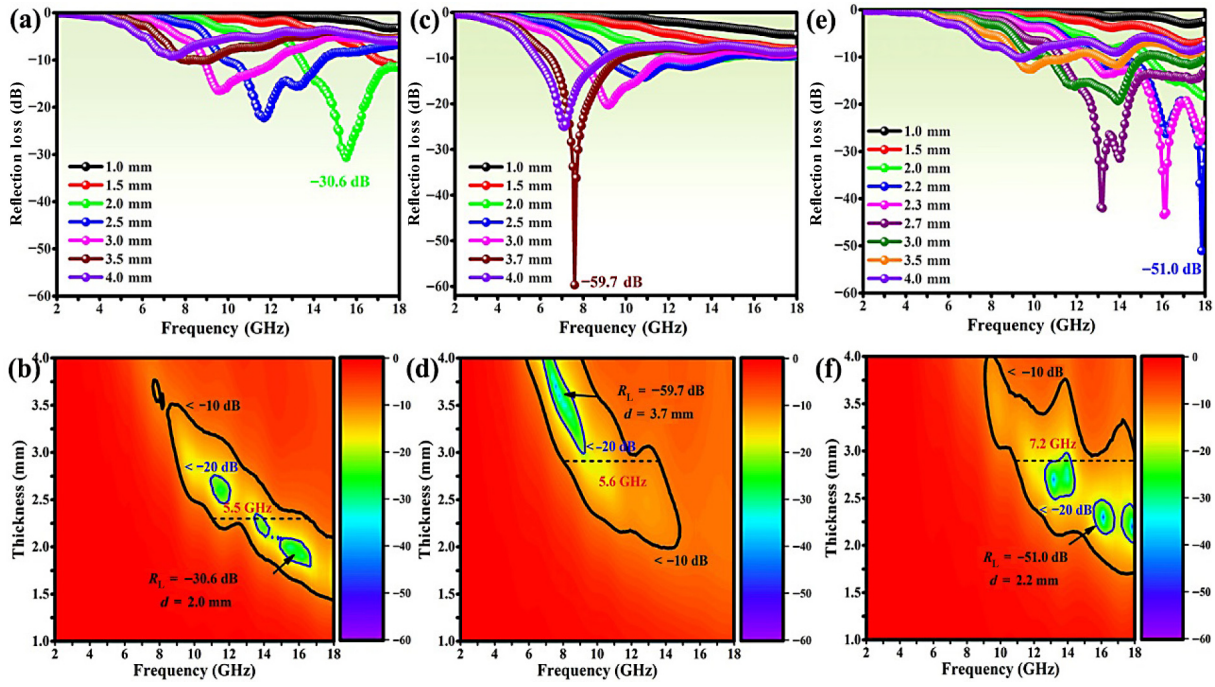

Figure 7 Reflection loss of PCSs (a) and (b), Co-PCSs (c) and (d) and CoNi-PCSs (e) and (f).

Through the above analysis, it can be concluded that the introduction of magnetic particles into PCSs can conspicuously improve microwave absorption performance of PCSs. The results are summarized in Table 1.

Table 1 Microwave absorption performances of PCSs, Co-PCSs and CoNi-PCSs.

Samples	Filler loading	R_{Lmin} / thickness	Effective bandwidth / thickness
PCSs	15 wt.%	−30.6 dB/2 mm	5.5 GHz/2.3 mm
Co-PCSs	15 wt.%	−59.7 dB/3.7 mm	5.6 GHz/2.9 mm
CoNi-PCSs	15 wt.%	−51 dB/2.2 mm	7.2 GHz/2.9 mm

3.6 Analyses of electromagnetic parameters

The relative complex permittivity ($\varepsilon_r = \varepsilon_r' - j\varepsilon_r''$) and the complex permeability ($\mu_r = \mu_r' - j\mu_r''$) are two important parameters that determining the final microwave absorption performance. In order to deeply analyze the the microwave absorption performance of PCSs, Co-PCSs and CoNi-PCSs, the electromagnetic parameters are tested in Fig. 8. Among them, ε' and μ' represent the storage capacity of dielectric loss and magnetic loss, respectively, and ε'' and μ'' represent the dissipation capacity of dielectric loss and magnetic loss, respectively. As shown in Fig. 8(a), the ε' values of all samples decrease with the increase of frequency, which is mainly due to the fact that the hysteresis of loss becomes more obvious at high frequencies [24]. Specifically, the ε' of PCSs decreases from 7.5 to 6.2, the ε' of Co-PCSs decreases from 7.2 to 2.7, and the ε' of CoNi-PCSs decreases from 4.9 to 3.6. From Fig. 8(b), it can be seen that the ε'' of PCSs is higher than that of Co-PCSs and CoNi-PCSs, which can be explained by the free electron theory ($\varepsilon'' = \sigma/(2\pi\varepsilon_0 f)$), where ε'' is proportional to the conductivity σ of the materials. Due to the nanoscale effect, the conductivity of magnetic Co and CoNi particles are significantly lower than that of carbon matrix. Therefore, after the addition of magnetic particles to PCSs, the conductivity of PCSs decreases, so the ε'' of PCSs is high [25]. Figure 8(c) shows the dielectric loss values of PCSs, Co-PCSs, and CoNi-PCSs. As depicted in Fig. 8(c), the dielectric losses of all samples exhibit a little difference in the range of 2–12 GHz, but the dielectric losses of Co-PCSs and CoNi-PCSs are significantly enhanced in the range of 12–18 GHz, which may be due to the addition of magnetic particles. A large number of heterogeneous interfaces can be formed between magnetic particles and carbon matrix, thereby improving the interfacial polarization [26]. Since there is no magnetic component in the PCSs, the μ' and μ'' values are constant. As shown in Fig. 8(d), due to the relaxation of the magnetic moment, the μ' of Co-PCSs and CoNi-PCSs decreases slightly, while the μ'' (Fig. 8(e)) and the $\tan\delta_\mu$ (Fig. 8(f)) show the similar trends. However, the higher μ'' and $\tan\delta_\mu$ values of CoNi-PCSs demonstrate that CoNi-PCSs possess higher magnetic loss than that of Co-PCSs.

Generally speaking, microwave absorption performances of materials are jointly determined by impedance matching and loss constant. Among them, impedance matching is a prerequisite for materials to have microwave absorption performances because only good impedance matching can enable electromagnetic waves to be incident into materials and thus be dissipated through various loss mechanisms [27, 28]. If the impedance matching of materials is poor, the electromagnetic waves will be reflected on the surface of materials and it is difficult for them to enter the interior of materials. The conductivity of PCSs is relatively high, and the impedance bandgap with air is large. Therefore, the impedance matching of PCSs is slightly lower than those of Co-PCSs and CoNi-PCSs. A higher the loss constant confirms a better microwave absorption performance. The losses include dielectric loss and magnetic loss [29]. In the range of 2–18 GHz, dielectric loss mainly comes from conduction loss, dipole polarization and interface polarization [30, 31]. Although the conductivity and conduction

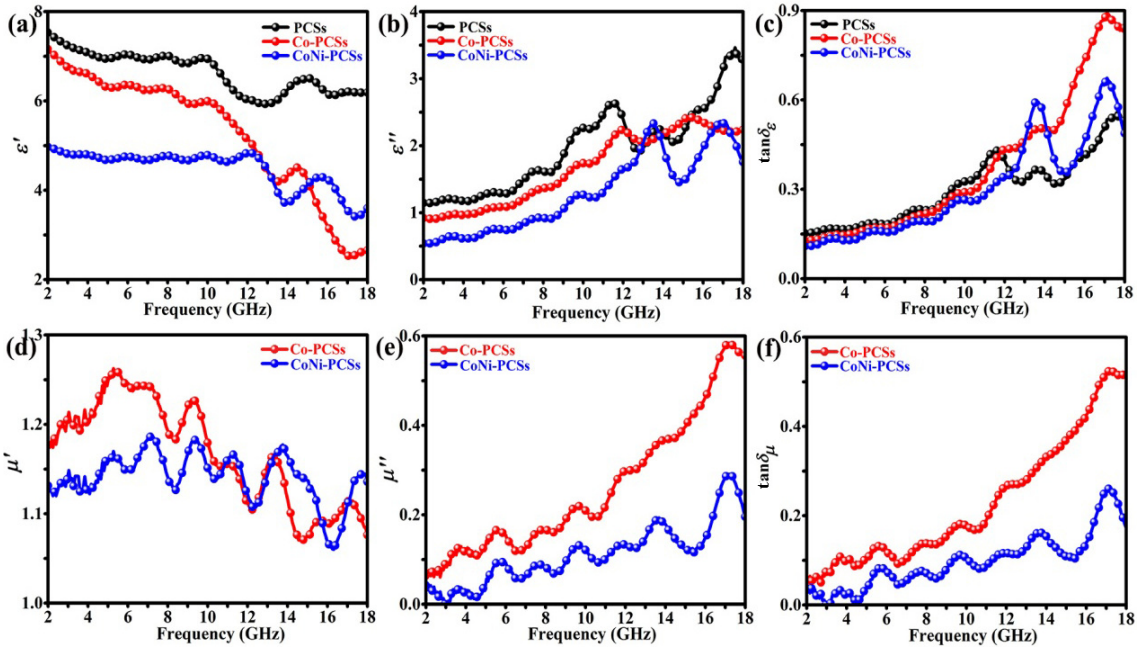

Figure 8 Electromagnetic parameters of PCSs, Co-PCSs and CoNi-PCSs.

loss of PCSs are higher, Co-PCSs and CoNi-PCSs have more abundant heterogeneous interfaces, thereby greatly enhancing the dipole polarization and interface polarization effects of the materials. The Debye relaxation theory is used to study the dipole polarization and interface polarization of PCSs, Co-PCSs and CoNi-PCSs, as shown in Eq. (3)

$$\left(\varepsilon' - \frac{\varepsilon_s + \varepsilon_\infty}{2}\right)^2 + (\varepsilon'') = \left(\frac{\varepsilon_s + \varepsilon_\infty}{2}\right)^2 \quad (3)$$

where the ε'–ε'' curve of materials should be a semicircle, defined as the Cole–Cole semicircle, and each semicircle represents a Debye relaxation process. As shown in Fig. 9, Co-PCSs and CoNi-PCSs have more Cole–Cole semicircles or irregular semicircles compared to PCSs, indicating that they have multiple polarization relaxation processes. This is mainly due to the formation of a large number of heterogeneous interfaces between the introduced magnetic particles and the carbon matrix. It is clear that the electrical characteristics vary at the heterointerfaces between magnetic particles and carbon matrix, the unbalanced charge density acts as the topological condition to produce capacitor-like structure and generates interfacial polarization with the synergistic effect of heterointerfaces. In the range of 2–18 GHz, magnetic losses of Co-PCSs and CoNi-PCSs are mainly determined by ferromagnetic resonance and eddy current loss. When $C_0 = \mu''(\mu')^{-2}f^{-1}$ is a constant, magnetic loss comes from eddy current loss [32]. As shown in Fig. 10(a), the C_0 values of Co-PCSs and CoNi-PCSs fluctuate significantly with the increase of frequency, indicating that both ferromagnetic resonance and eddy current loss contribute to the magnetic loss. The attenuation constants (α) of PCSs, Co-PCSs and CoNi-PCSs are calculated using Eq. (4).

$$\alpha = \frac{\sqrt{2}\pi f}{c}\sqrt{(\mu''\varepsilon'' - \mu'\varepsilon') + \sqrt{(\mu''\varepsilon'' - \mu'\varepsilon')^2 + (\mu'\varepsilon'' + \mu''\varepsilon')^2}} \quad (4)$$

As shown in Fig. 10(b), the attenuation constant α of Co-PCSs is significantly higher than that of PCSs throughout the entire frequency range, indicating that the microwave absorption performance of Co-PCSs is higher than that of PCSs. However, for CoNi-PCSs, the attenuation constant α does not differ much from that of PCSs, but the wave absorption performance of CoNi-PCSs is significantly higher than that of PCSs. This is mainly due to the fact that CoNi-PCSs have better impedance matching, which is more conducive to the incident electromagnetic waves entering the materials and being dissipated [33].

The microwave absorption mechanism of PCSs, Co-PCSs and CoNi-PCSs is shown in Fig. 11. Firstly, heteroatoms, disordered

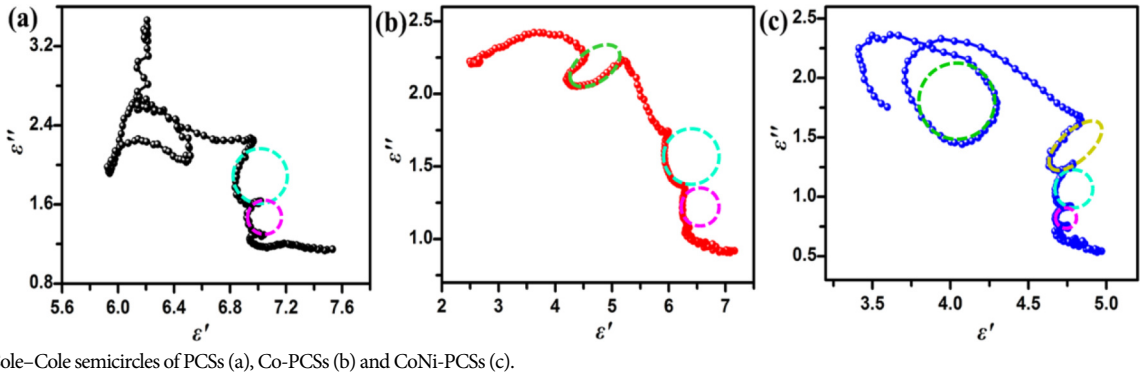

Figure 9 Cole–Cole semicircles of PCSs (a), Co-PCSs (b) and CoNi-PCSs (c).

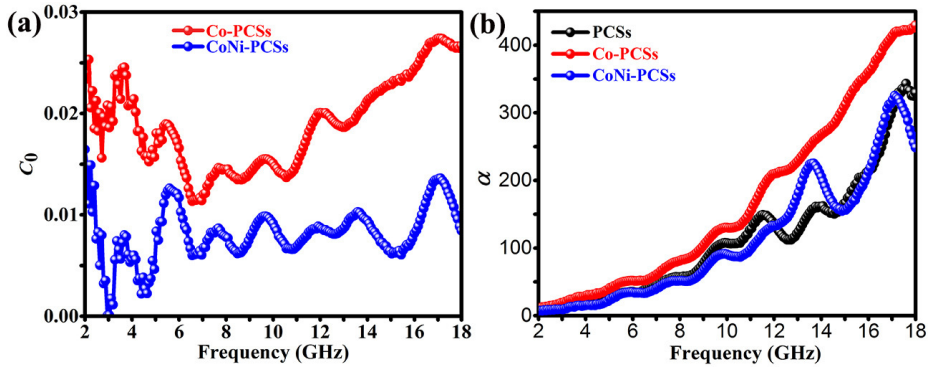

Figure 10 C_0 (a) and α (b) values of PCSs, Co-PCSs and CoNi-PCSs.

carbon frameworks and defects/metal vacancies are prone to generating dipole polarization and defect polarization; interfaces are easily induced between magnetic particles and carbon matrices and different forms of carbon structures, such as graphite-amorphous carbon, Co-C and CoNi-C, both of them are conducive to improve dielectric loss of absorbent. Secondly, compared with PCSs, which only own dielectric loss, the introduction of magnetic particles not only provides magnetic loss, but also improves the matching impedance and microwave absorption performance of the materials through multi-loss synergy. Finally, the porous structure is conducive to regulating dielectric constant of materials and reducing its filling amount in paraffin, thereby achieving lightweight and efficient microwave absorption performance.

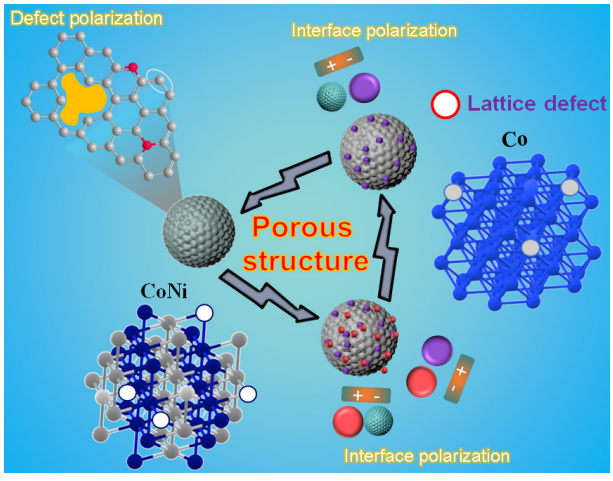

Figure 11 Microwave absorption mechanism of PCSs, Co-PCSs and CoNi-PCSs.

4 Conclusions

Magnetic porous carbon spheres Co-PCSs and CoNi-PCSs prepared by high-temperature carbonization and anchoring different metal ions in poly-(tannin acid) spheres using the formaldehyde-assisted ligand cross-linking strategy have lightweight and efficient microwave absorption properties. By changing chemical composition of magnetic particles, the microwave absorption intensity and effective frequency bandwidths of materials can be regulated. When the filling amount of absorbent is 15 wt.%, the minimum reflection loss of Co-PCSs is −59.7 dB at a thickness of 3.7 mm, while the effective frequency bandwidth of CoNi-PCSs reaches 7.2 GHz with thickness of 2.9 mm. Its excellent microwave absorption performance is attributed to following aspects. (1) The introduction of magnetic particles can not only improve impedance matching of materials, but also enhance magnetic loss. (2) A large number of heterogeneous interfaces are formed between magnetic particles and carbon matrix, which is conducive to improving the interface polarization effect. (3) The electromagnetic synergy between magnetic loss and dielectric loss is conducive to achieving broadband absorption characteristics. The expected research results will provide an idea for the preparation of lightweight and efficient microwave absorption materials.

Data availability

All data needed to support the conclusions in the paper are presented in the manuscript and the Electronic Supplementary Material. Additional data related to this paper may be requested from the corresponding author upon request.

Acknowledgements

This work was financially supported by the National Natural Science Foundation of China (No. 52373271). The authors would like to thank Zhang San from Shiyanjia Lab (www.shiyanjia.com) for the VSM analysis.

Declaration of competing interest

All the contributing authors report no conflict of interests in this work.

Author contribution statement

J. D.: Data curation, project administration, validation, writing manuscript, experimental design. P. B. L.: Data curation, funding acquisition, experimental design.

Use of AI statement

None.

References

[1] Xiang, Z.; Shi, Y. Y.; Zhu, X. J.; Cai, L.; Lu, W. Flexible and waterproof 2D/1D/0D construction of MXene-based nanocomposites for electromagnetic wave absorption, EMI shielding, and photothermal conversion. *Nano-Micro Lett.* **2021**, *13*, 150.

[2] Guo, Y. Q.; Ruan, K. P.; Wang, G. S.; Gu, J. W. Advances and mechanisms in polymer composites toward thermal conduction and electromagnetic wave absorption. *Sci. Bull.* **2023**, *68*, 1195–1212.

[3] Xu, H. X.; Zhang, G. Z.; Wang, Y.; Wang, Y. R.; Wang, H. L.;

Huang, Y.; Liu, P. B. Heteroatoms-doped carbon nanocages with enhanced dipolar and defective polarization toward light-weight microwave absorbers. *Nano Res.* **2022**, *15*, 8705–8713.

[4] Wu, Z. C.; Cheng, H. W.; Jin, C.; Yang, B. T.; Xu, C. Y.; Pei, K.; Zhang, H. B.; Yang, Z. Q.; Che, R. C. Dimensional design and core-shell engineering of nanomaterials for electromagnetic wave absorption. *Adv. Mater.* **2022**, *34*, 2107538.

[5] Zhang, Y. L.; Ruan, K. P.; Zhou, K.; Gu, J. W. Controlled distributed $Ti_3C_2T_x$ hollow microspheres on thermally conductive polyimide composite films for excellent electromagnetic interference shielding. *Adv. Mater.* **2023**, *35*, 2211642.

[6] Liu, P. B.; Gao, S.; Liu, X. D.; Huang, Y.; He, W. J.; Li, Y. T. Rational construction of hierarchical hollow CuS@CoS_2 nanoboxes with heterogeneous interfaces for high-efficiency microwave absorption materials. *Compos. Part, B: Eng.* **2020**, *192*, 107992.

[7] Sun, M. X.; Wang, D. R.; Xiong, Z. M.; Zhang, Z. W.; Qin, L.; Chen, C. C.; Wu, F.; Liu, P. B. Multi-dimensional Ni@C-CoNi composites with strong magnetic interaction toward superior microwave absorption. *J. Mater. Sci. Technol.* **2022**, *130*, 176–183.

[8] Liu, P. B.; Gao, S.; Wang, Y.; Zhou, F. T.; Huang, Y.; Luo, J. H. Metal-organic polymer coordination materials derived Co/N-doped porous carbon composites for frequency-selective microwave absorption. *Compos. Part, B: Eng.* **2020**, *202*, 108406.

[9] Wang, F. Y.; Liu, Y. L.; Zhao, H. H.; Cui, L. R.; Gai, L. X.; Han, X. J.; Du, Y. C. Controllable seeding of nitrogen-doped carbon nanotubes on three-dimensional Co/C foam for enhanced dielectric loss and microwave absorption characteristics. *Chem. Eng. J.* **2022**, *450*, 138160.

[10] Liu, D. W.; Yang, L.; Wang, F. Y.; Zhang, H.; Liu, J.; Lv, T.; Zhao, H. J.; Du, Y. C. Hierarchical carbon nanotubes@Ni/C foams for high-performance microwave absorption. *Carbon* **2022**, *196*, 867–876.

[11] Wu, Y.; Zhao, Y.; Zhou, M.; Tan, S. J.; Peymanfar, R.; Aslibeiki, B.; Ji, G. B. Ultrabroad microwave absorption ability and infrared stealth property of nano-micro CuS@rGO lightweight aerogels. *Nano-Micro Lett.* **2022**, *14*, 171.

[12] Zhao, H. H.; Xu, X. Z.; Wang, Y. H.; Fan, D. G.; Liu, D. W.; Lin, K. F.; Xu, P.; Han, X. J.; Du, Y. C. Heterogeneous interface induced the formation of hierarchically hollow carbon microcubes against electromagnetic pollution. *Small* **2020**, *16*, 2003407.

[13] Ding, D.; Wang, Y.; Li, X. D.; Qiang, R.; Xu, P.; Chu, W. L.; Han, X. J.; Du, Y. C. Rational design of core-shell Co@C microspheres for high-performance microwave absorption. *Carbon* **2017**, *111*, 722–732.

[14] Liu, P. B.; Gao, S.; Zhang, G. Z.; Huang, Y.; You, W. B.; Che, R. C. Hollow engineering to Co@N-doped carbon nanocages via synergistic protecting-etching strategy for ultrahigh microwave absorption. *Adv. Funct. Mater.* **2021**, *31*, 2102812.

[15] Zhang, X. C.; Li, B.; Xu, J.; Zhang, X.; Shi, Y. N.; Zhu, C. L.; Zhang, X. T.; Chen, Y. J. Metal ions confined in periodic pores of MOFs to embed single-metal atoms within hierarchically porous carbon nanoflowers for high-performance electromagnetic wave absorption. *Adv. Funct. Mater.* **2023**, *33*, 2210456.

[16] Liu, P. Z.; Gao, T. D.; He, W. J.; Liu, P. B. Electrospinning of hierarchical carbon fibers with multi-dimensional magnetic configurations toward prominent microwave absorption. *Carbon* **2023**, *202*, 244–253.

[17] Wang, H. Y.; Sun, X. B.; Wang, G. S. A MXene-modulated 3D crosslinking network of hierarchical flower-like MOF derivatives towards ultra-efficient microwave absorption properties. *J. Mater. Chem. A* **2021**, *9*, 24571–24581.

[18] Zhang, Y.; Yang, Z. H.; Li, M.; Yang, L. J.; Liu, J. C.; Ha, Y.; Wu, R. B. Heterostructured CoFe@C@MnO2 nanocubes for efficient microwave absorption. *Chem. Eng. J.* **2020**, *382*, 123039.

[19] Wu, Z. C.; Tian, K.; Huang, T.; Hu, W.; Xie, F. F.; Wang, J. J.; Su, M. X.; Li, L. Hierarchically porous carbons derived from biomasses with excellent microwave absorption performance. *ACS Appl. Mater. Interfaces* **2018**, *10*, 11108–11115.

[20] Wang, H. G.; Meng, F. B.; Li, J. Y.; Li, T.; Chen, Z. J.; Luo, H. B.; Zhou, Z. W. Carbonized Design of hierarchical porous carbon/Fe_3O_4@Fe derived from loofah sponge to achieve tunable high-performance microwave absorption. *ACS Sustainable Chem. Eng.* **2018**, *6*, 11801–11810.

[21] Xiang, Z.; Song, Y. M.; Xiong, J.; Pan, Z. B.; Wang, X.; Liu, L.; Liu, R.; Yang, H. W.; Lu, W. Enhanced electromagnetic wave absorption of nanoporous Fe_3O_4 @ carbon composites derived from metal-organic frameworks. *Carbon* **2019**, *142*, 20–31.

[22] Zhang, Y. L.; Kong, J.; Gu, J. W. New generation electromagnetic materials: Harvesting instead of dissipation solo. *Sci. Bull.* **2022**, *67*, 1413–1415.

[23] Ge, C. Q.; Wang, L. Y.; Liu, G. Research progress in carbon-based/carbonyl iron composite microwave absorption materials. *J. Mater. Eng.* **2019**, *47*, 43–54.

[24] Xiang, L. L.; Qi, X. S.; Rao, Y. C.; Wang, L.; Gong, X.; Chen, Y. L.; Peng, Q.; Zhong, W. A simple strategy to develop heterostructured carbon paper/Co nanoparticles composites with lightweight, tunable and broadband microwave absorption. *Mater. Today Phys.* **2023**, *34*, 101030.

[25] Wen, C. Y.; Li, X.; Zhang, R. X.; Xu, C. Y.; You, W. B.; Liu, Z. W.; Zhao, B.; Che, R. C. High-density anisotropy magnetism enhanced microwave absorption performance in $Ti_3C_2T_x$ MXene@Ni microspheres. *ACS Nano* **2021**, *16*, 1150–1159.

[26] Zhao, T. B.; Jia, Z. R.; Zhang, Y.; Wu, G. L. Multiphase molybdenum carbide doped carbon hollow sphere engineering: The superiority of unique double-shell structure in microwave absorption. *Small* **2023**, *19*, 2206323.

[27] Du, Z. B.; Shi, S. Q.; Chen, Y. B.; Chu, H. R.; Yang, C. Research progress in dielectric graphene microwave absorbing composites. *J. Mater. Eng.* **2022**, *50*, 74–84.

[28] Zhong, X.; He, M. K.; Zhang, C. Y.; Guo, Y. Q.; Hu, J. W.; Gu, J. W. Heterostructured BN@Co-C@C endowing polyester composites excellent thermal conductivity and microwave absorption at C band. *Adv. Funct. Mater.* **2024**, *34*, 2313544.

[29] Li, C.; Peng, Q.; Qi, X. S.; Chen, Y. L.; Gong, X.; Wang, X.; Deng, C. Y.; Zhong, W.; Du, Y. W. Morphology optimization strategy of flower-like $CoNi_2S_4$/Co_9S_8@MoS_2 core@shell nanocomposites to achieve extraordinary microwave absorption performances. *J. Colloid Interface Sci.* **2022**, *606*, 1128–1139.

[30] Zhang, Z. W.; Cai, Z. H.; Wang, Z. Y.; Peng, Y. L.; Xia, L.; Ma, S. P.; Yin, Z. Z.; Huang, Y. A review on metal-organic framework-derived porous carbon-based novel microwave absorption materials. *Nano-Micro Lett.* **2021**, *13*, 56.

[31] He, M. K.; Hu, J. W.; Yan, H.; Zhong, X.; Zhang, Y. L.; Liu, P. B.; Kong, J.; Gu, J. W. Shape Anisotropic chain-like CoNi/polydimethylsiloxane composite films with excellent low-frequency microwave absorption and high thermal conductivity. *Adv. Funct. Mater.*, in press, DOI: 10.1002/adfm.202316691.

[32] Wang, H. Y.; Sun, X. B.; Yang, S. H.; Zhao, P. Y.; Zhang, X. J.; Wang, G. S.; Huang, Y. 3D ultralight hollow NiCo compound@MXene composites for tunable and high-efficient microwave absorption. *Nano-Micro Lett.* **2021**, *13*, 206.

[33] He, Z. Z.; Xu, H. X.; Shi, L. Z.; Ren, X. R.; Kong, J.; Liu, P. B. Hierarchical Co_2P/CoS_2@C@MoS_2 composites with hollow cavity and multiple phases toward wideband electromagnetic wave absorption. *Small* **2024**, *20*, 2306253.